Dynamic Response of Stereoblock Elastomeric Polypropylene Studied by Rheooptics and X-ray Scattering. 1. Influence of Isotacticity

Willy Wiyatno,[†] John A. Pople,[‡] Alice P. Gast,[§] Robert M. Waymouth,*[,⊥] and Gerald G. Fuller*[,†]

Chemical Engineering Department, Stanford University, Stanford, California 94305; Stanford Synchrotron Radiation Laboratory, Stanford Linear Accelerator Center, Stanford University, Stanford, California 94309; Chemical Engineering Department, Massachusetts Institute of Technology, Cambridge, Massachusetts 02139; and Department of Chemistry, Stanford University, Stanford, California 94305

Received February 19, 2002; Revised Manuscript Received July 1, 2002

ABSTRACT: The dynamic response of elastomeric polypropylene (ePP) prepared by metallocene 2-arylindene hafnium catalyst was investigated by rheooptical birefringence as well as wide- and small-angle X-ray scattering (WAXS and SAXS). Solvent extraction of ePP ([mmmm] = 34%) results in three fractions with increasing tacticity, crystallinity, and molecular weight in the following order: ether soluble ([mmmm] = 21%), heptane soluble (44%), and heptane insoluble (76%). Unstretched ePP reveals a crystalline phase of the α-form isotactic polypropylene (i-PP). Tensile stretching of ePP yields three sets of scatterings (equatorial, off-axis diagonal, and meridional arc). High-tacticity fractions contribute to the equatorial and off-axis diagonal scatterings, revealing molecular-scale orientation parallel to the strain axis and crystalline phase transformation from the α-form to the mesomorphic form. The meridional arc is contributed by the low-tacticity ether-soluble fraction with crystalline chains oriented with a preferred direction orthogonal relative to the strain direction. SAXS, which probes long-range ordering, exhibits a broad and diffuse meridional peak for the intermediate-tacticity fraction. This implies that lamellae are oriented orthogonal to the strain direction upon stretching. Permanent deformation of ePP after stretching, as measured by the residual strain (tensile set), originates from permanently oriented crystallites and chains pinned within crystalline networks.

Introduction

The advent of homogeneous metallocene polymerization catalysts has produced a variety of homo- and copolymer of poly-(α-olefins) with tailored structures and physical properties.[1−3] Propylene polymerization using these catalysts has produced controlled architecture of polypropylenes such as isotactic,[4−6] syndiotactic,[4,5,7] heterotactic,[4,5] and stereoblock microstructures.[8−10] Elastomeric polypropylene was first synthesized by Natta using heterogeneous Ziegler-type catalysts.[11,12] He attributed the elastomeric behavior to their low crystallinity and blocks of alternating isotactic crystalline and atactic amorphous segments. After Natta's work there have been various reports of related materials produced with different catalysts.[1−3] Collette and co-workers demonstrated that elastomeric polypropylenes could be obtained using supported tetraalkyl group IVB catalysts.[13−15] Chien and co-workers reported the first metallocene catalyst to produce elastomeric polypropylenes using chiral, stereorigid *ansa*-titanocene catalysts.[16−18] Collins and co-workers described the synthesis of elastomeric polypropylenes using 3-methyl-substituted *ansa*-sirconocene catalysts.[19−21] More recently, several classes of metallocene catalysts have been developed for the production of elastomeric polypropylenes.[22−35]

Our group has reported that metallocene catalysts derived from 2-arylindene ligands produced elastomeric polypropylenes which could be separated into fractions differing in tacticity and crystallinity.[8,10,36−39] Morphological investigation of these low-crystallinity materials exhibited morphology reminiscent of classical semicrystalline polymers showing lamellae and crosshatched lamellae which could organize into hedrites and spherulites depending on thermal history and crystallinity.[40]

In the current study, we examined the dynamic response of elastomeric polypropylene derived from 2-arylindene metallocene catalyst with a hafnium precursor. A combination of rheooptical birefringence, X-ray scattering, and tensile stress techniques was used to probe the dynamic response of the materials to tensile and shear deformations. The birefringence yields information on deformation-induced anisotropy arising from both oriented amorphous chains and crystallites. The X-ray scattering offers complementary information about the response of the crystalline regions to deformation. Wide- and small-angle X-ray scattering (WAXS and SAXS, respectively) reveal short- and long-range ordering as well as the crystalline form of the materials.[41,42]

In the first paper of this series, we present the room temperature dynamic response of the whole ePP and its solvent fractions under uniaxial extensional deformation. Simultaneous tensile stress and birefringence offer insight into the relaxation dynamics and the origin of the tensile set (permanent deformation). The crystalline response, as probed by WAXS, provides data pertaining to crystalline phase transformation and the crystalline relaxation. The role of each solvent fraction (low-, intermediate-, and high-tacticity fractions) is investigated to probe the effect of tacticity and crystallinity on deformation. In the second paper of this series, the unusual dynamic response of the low-tacticity fraction is discussed in detail. Rheooptical birefringence and WAXS were employed to follow the dynamic response of the neat low-tacticity fraction subjected to

[†] Chemical Engineering Department, Stanford University.
[‡] Stanford Linear Accelerator Center, Stanford University.
[§] Massachusetts Institute of Technology.
[⊥] Department of Chemistry, Stanford University.

10.1021/ma020261o CCC: $22.00
Published on Web 09/18/2002

Table 1. Polymer Characterization

sample	wt %	M_w [a] ($\times 10^{-3}$)	PDI[a]	mmmm (%)[b]	m (%)[b]	IR index[c]	T_m (°C)[d]	ΔH (J/g)[d]	crystallinity% DSC	crystallinity% XRD
ePP-10	100	201	2.3	34	73	0.34	42−149	22	11	8
ES-ePP10	48	147	2.1	21	67	0.19	41−45	2	1	2
HS-ePP10	42	220	2.3	44	79	0.38	42	32	15	11
HI-ePP10	10	432	2.5	76	92	0.70	47−155	82	39	37

[a] Determined by GPC (Waters, 150 °C) at BP Chemical Co. [b] Determined by ^{13}C NMR. [c] Determined by the ratio of absorbance intensity A_{998}/A_{975}. [d] Determined by DSC endotherm scan from 0 to 200 °C at 20 °C/min.

uniaxial extensional and step-shear deformations. The role of the low-tacticity fraction when blended with higher-tacticity fractions is also analyzed in the context of the dynamic response under deformation.

Experimental Section

Materials. The elastomeric polypropylene (ePP-10) was synthesized by BP Chemical Co. in liquid propylene at 50 °C with bis(2-(3,5-di-*tert*-butylphenyl)indenyl)hafnium dichloride as reported elsewhere.[43] ^{13}C NMR sequence analysis indicated [m] = 72.9%, [mm] = 54.8%, and [mmmm] = 34.0%. Molecular weight analysis by GPC specified M_w = 201 000 and M_w/M_n = 2.3. The melt flow rate was 10.6 g/10 min at 230 °C with 2.16 kg load.

Solvent extraction was carried out by successive extraction of ePP-10 with boiling diethyl ether and heptane under a nitrogen environment following the procedure reported previously.[10] A 500 mL round-bottom flask, attached to a Kumagawa extractor, was charged with 300 mL of solvent added with 0.2 wt % antioxidant 2,6-di-*tert*-butyl-4-methylphenol (BHT). Polymer (∼10 g) was packed into a thimble layered with a plug of glass wool. Extraction was conducted for 24 h with a heating rate such that the flushing frequency of the extractor was 4−5 min/flush. After the extraction, polymer was precipitated in acidified methanol (3000 mL, 1% HCl) with vigorous stirring. The extraction was repeated twice for each solvent. The precipitated polymers were then dried in a vacuum for at least 1 day.

Uniaxial Extensional Deformation. Tensile stretching was conducted with a Miniature Material Tester, MiniMat 2000 (Rheometric Scientific, Inc.), at room temperature using ASTM D-1708 dumbbell specimens with a gauge length of 2.2 cm. Specimens were die-cut from compression-molded sheets (∼0.5 mm thickness) pressed at 180 °C in a hot press (model C, Carver, Menomone Falls, WI) and slowly cooled to room temperature. The crosshead separation rate for elongation and contraction was 1.0 and 0.1 mm/min, respectively. The (true) tensile stress (σ) was calculated as the ratio of tensile force (F) to the instantaneous cross-sectional area (A) interpolated from caliper measurements: $\sigma = F/A$. The strain (ϵ) was computed from the ratio of the change in separation distance between two lines ($\Delta l = l - l_0$) drawn at the middle of the specimen to its original separation distance (l_0): $\epsilon = \Delta l/l_0$. The degree of permanent deformation was measured in tensile set, which was the residual strain of the sample following a deformation.

Dynamic Birefringence. The dynamic response of the materials was probed with optical polarimetry following the time-dependent birefringence of a deformed sample using the optical train setup whose schematic is shown in Figure 1. In the optical setup, monochromatic HeNe light (632.8 nm) passed through a polarizer (0°) and a photoelastic modulator (PEM, 45°) before it was transmitted through a sample with a normal incidence. The transmitted light then passed through an analyzing polarizer (45°) and impinged upon a photodiode detector where the signals were demodulated using lock-in amplifiers. The intensity of the transmitted beam is[44]

$$I = \frac{I_0}{4}[1 + 2J_1(A)\sin(\omega t)\sin(\delta')] \quad (1)$$

$$\delta' = \frac{2\pi d\Delta n}{\lambda} \quad (2)$$

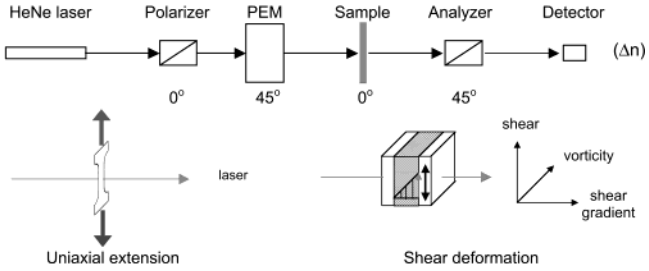

Figure 1. Rheooptical birefringence setup and the Cartesian geometries defining the uniaxial extensional and shear deformations.

where I_0 is the incident beam intensity, $J_1(A)$ is a calibration constant determined experimentally using elements of known retardation, ω is the modulation frequency of the photoelastic modulator (PEM), δ' is the retardation of the sample, d is the sample thickness, λ is the wavelength of the laser, and Δn is the birefringence of the stretched samples. In uniaxial extensional deformation, the sample thickness d was measured at some intervals of strain and interpolated between these intervals.

Wide- and Small-Angle X-ray Scattering (WAXS and SAXS). WAXS and SAXS experiments were performed at beamline 1-4 of the Stanford Synchrotron Radiation Laboratory (SSRL). The X-ray source has a flux $\sim 10^{10}$ photons at a wavelength of λ = 1.488 Å. A CCD area detector (Photonic Science) was used to collect the 2-D diffraction data: the detector has an active area of 100 mm diameter, which is mapped via a tapered fiber-optic bundle to the CCD chip with a 1024 × 1024 array of 25 μm square pixels. In the WAXS experiments, 2-D images were assembled from the summation of 1000 consecutive frames, and the portion of reciprocal space was calibrated with a Lupolen standard. The 2-D scattering images of the SAXS were assembled from 20 000 consecutive frames and were calibrated with a chicken tendon. Sample-to-detector distances for WAXS and SAXS were 10 and 110 cm, respectively. Data analysis was performed using 1-D profiles integrated either azimuthally or radially from the 2-D patterns and corrected for background scattering and scattering from windows associated with the optics. The scattering vector q follows the relationship $q = (4\pi/\lambda)\sin(\theta)$, in which θ is the scattering angle and θ is the wavelength of the X-ray. In morphological studies, the scattering angle 2θ is more widely used to represent the scattering vector q, which is derived from the above equation.[45] Azimuthal scans were performed by integrating the intensity over a narrow band of scattering angle (2θ) as a function of azimuthal angles.

Results

Elastomeric Polypropylene (ePP-10). The characterization of the elastomeric polypropylene (ePP) and its solvent fraction is given in Table 1. Tensile property investigation, reported elsewhere,[46] revealed that the whole ePP with tacticity [mmmm] = 34% exhibited elastomeric tensile properties with a tensile strength of 8 MPa, a strain to break of 1300%, and good elastic recoveries as measured by a moderate tensile set of 58% elongation (after stretching the sample to 300% elongation). As mentioned previously, the parent ePP could

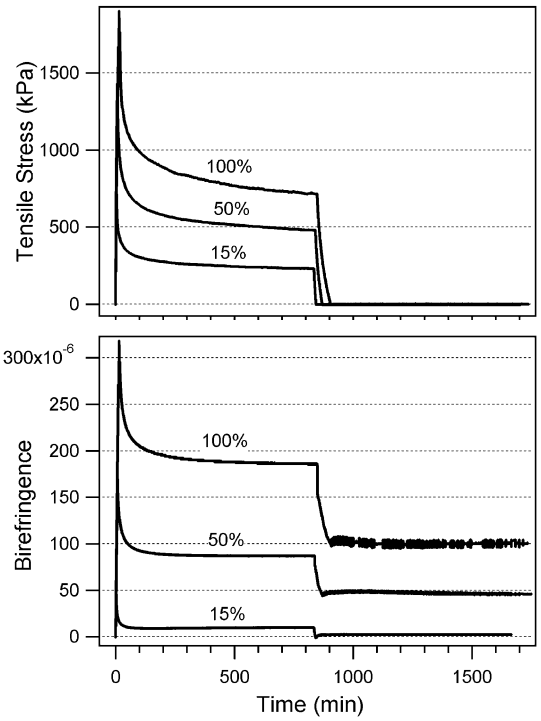

Figure 2. Simultaneous tensile stress and birefringence response of elastomeric polypropylene ePP-10 under various strains. All samples followed the following procedure: (1) elongation at 10 mm/min to a specified strain, (2) hold at strain for 14 h, (3) retraction (reversed elongation) at 1 mm/min to zero stress, and (4) maintained zero stress by adjusting strain.

be extracted with solvent boiling fractionation into three fractions differing in average tacticity, crystallinity, and molar mass. The fraction soluble in boiling ether has the lowest tacticity (ES-ePP10, [mmmm] = 21%), comprising 48 wt % of ePP-10. The remaining ether-insoluble portion could be further extracted in boiling heptane to yield an intermediate-tacticity heptane-soluble fraction (HS-ePP10, 42%) and a high-tacticity heptane-insoluble (HI-ePP10, 10%) fraction with average tacticities [mmmm] of 44% and 76%, respectively. The tensile properties of the low-tacticity fraction (ES) indicated that it was a weak gum elastomer, with behavior similar to those of atactic PP. The high-tacticity fraction (HI), on the other hand, behaved like a typical isotactic PP that deforms plastically and necks upon stretching. The intermediate-tacticity fraction (HS) exhibited elastomeric properties similar to the whole ePP but with a higher tensile modulus and better elastic recovery.

The results of the simultaneous tensile stress and birefringence of the whole ePP are shown in Figure 2. During tensile stretching (1 mm/min), both the tensile stress and birefringence increased to positive values. Since polypropylene has a positive stress−optical coefficient, a positive birefringence corresponds to polymer chains oriented parallel to the strain axis.[47,48] Once the desired strain was attained, the sample was held for 14 h to follow the relaxation dynamics of both the tensile stress and birefringence, which relaxed to positive values. As expected, the maximum and plateau values of both birefringence and stress after 14 h relaxation increased with increasing strain, as shown in Figure 3.

To investigate the origin of elasticity and tensile set, the stretched specimen (after 14 h under strain) was brought to zero stress by contracting the sample at 0.1

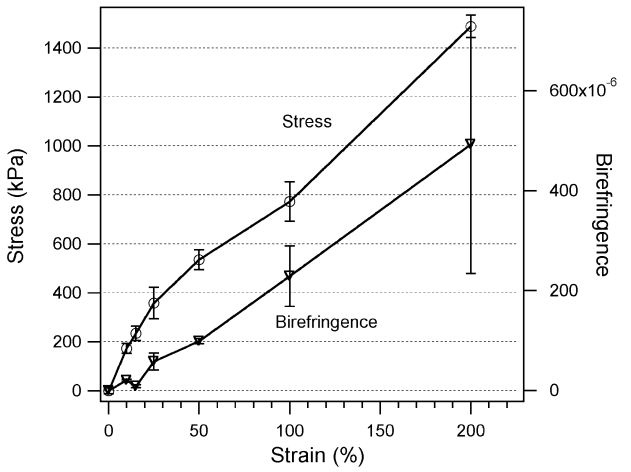

Figure 3. Stress and birefringence plateaus of ePP-10 at various strains.

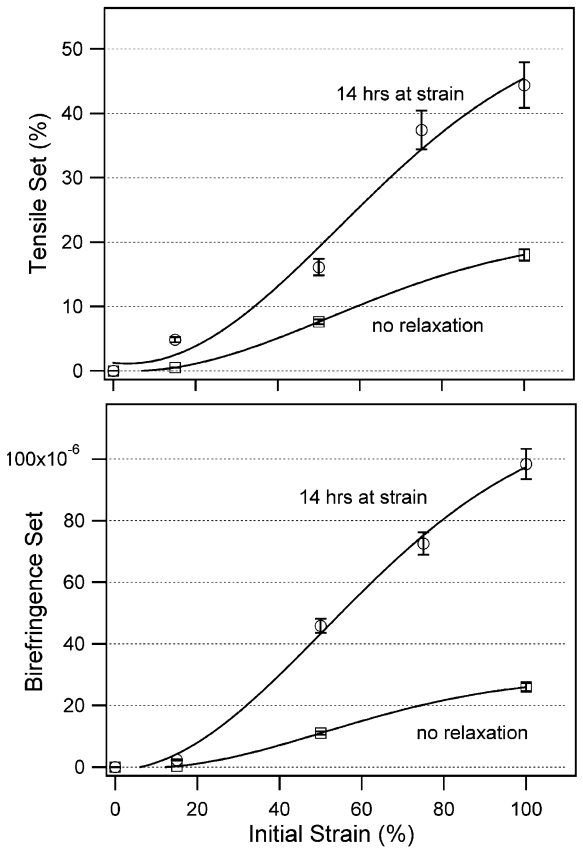

Figure 4. Tensile set and birefringence set of ePP-10 after complete relaxation of strain (zero stress) following two types of strain history: 14 h relaxation at constant strain or after an immediate recovery following the deformation.

mm/min (Figure 2). Once the sample reached zero stress during contraction, the elongation of the sample was adjusted automatically to maintain zero stress for another 14 h. The postdeformed sample was brought to the extent of an attainable recovery such that permanent deformation properties could be assessed. The residual strain (tensile set) and birefringence, as shown in Figure 4, suggested that a complete recovery was not achieved following the release of stress. The tensile set and residual birefringence increased with increasing initial strain. This phenomenon implied that higher degree of deformation resulted in a higher permanent

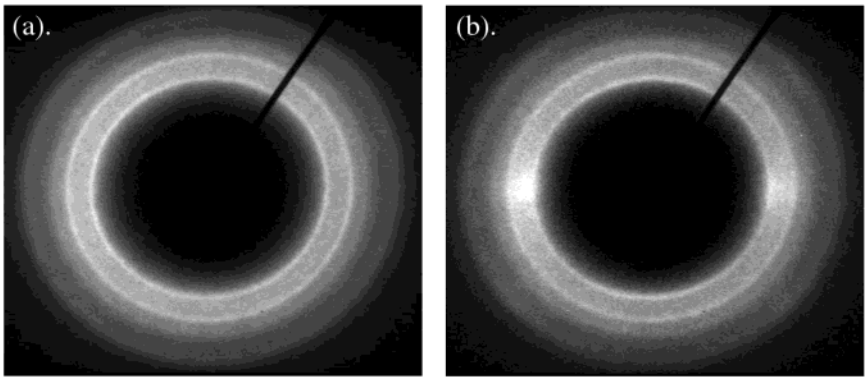

Figure 5. 2-D WAXS patterns of ePP: (a) before deformation and (b) at 300% strain with a vertical strain axis.

deformation in the thermoplastic elastomeric polypropylene.

Further investigation of the origin of the tensile set was carried out by varying the strain history prior to the release of stress. Specimens that were immediately brought back to zero stress (without undergoing stress relaxation) exhibited lower tensile set and residual birefringence (Figure 4). The discrepancy of the residual strain and birefringence between those of different strain history became larger with increasing strain, and hence the degree of permanent deformation correlated with elongation and strain history.

In addition to rheooptical measurements, deformation-induced anisotropy was probed by X-ray scattering methods. Figure 5 shows the 2-D wide-angle X-ray scattering (WAXS) of ePP at 0% and 300% strain. Unstretched ePP displayed isotropic crystalline rings typical of an α-form isotactic PP with three strong scattering peaks indexed as the (110), (040), and (130) reflections as well as a diffuse reflection of the (111) and (−131) planes.[40,49] Tensile stretching resulted in three sets of scatterings (along the equatorial, meridian, and diagonal axis), the intensities of which increased with increasing strain. The scattering along the equatorial axis, which is typical in stretched semicrystalline polymers, denoted polymer chains oriented parallel to the strain axis. The equatorial scattering exhibited a diffuse hump that is characteristic of the oriented mesomorphic form, not the distinct $\{hk0\}$ reflections of the oriented α-form.[50] Along the diagonal axis, a diffuse weak scattering was observed. The diffuse equatorial hump and the off-axis diagonal scattering are often regarded as the fingerprints of the mesomorphic form of isotactic PP, denoting a crystalline phase transformation upon deformation.[51,52] An unusual behavior was detected along the meridian axis. An increase in intensity was seen at the (110) scattering reflections (arcing) that implied crystalline chains orientation orthogonal to the strain direction.

The degree of molecular anisotropy with deformation was analyzed by plotting the azimuthal intensity integrated along a narrow band centered at the (110) scattering peaks ($13.4° \leq 2\theta \leq 14.6°$). As shown in Figure 6, higher molecular chain orientation appeared at increasing strain. Two sets of scatterings were evident from the azimuthal plots: strong equatorial scattering centered at 0° and 180° along with faint and broad meridional arc centered at 90° and 270°. It should be noted that the (110) azimuthal slices along the equatorial axis (0° and 180°) may contain both oriented mesomorphic form as well as oriented α-form since the scattering of the two forms are in general overlapping.

The relaxation dynamics, as probed by WAXS, exhibited an insignificant change in crystalline anisotropy following 1 h stress relaxation at 300% strain. The constant level of anisotropy suggested that crystalline regions did not relax appreciably. Hence, the relaxation observed in both tensile stress and birefringence could primarily be attributed to the dynamics of the amorphous chains. WAXS data suggested that on the short length scale (∼10 Å) molecular-scale chain orientation did not change while under strain. After the stress on ePP was released, the anisotropy observed by WAXS disappeared.

Solvent Fractions. 1. Heptane-Soluble (HS) Fraction. A WAXS profile of the intermediate-tacticity (HS) fraction is shown in Figure 7. The unstretched HS exhibited isotropic crystalline rings typical of the α-phase isotactic PP, similar to those of the whole ePP, with sharper scattering peaks due to its higher tacticity and crystallinity.[40] The stretched HS displayed two sets of scatterings that were also observed in ePP: equatorial and off-axis diagonal scatterings. The equatorial scattering contained a diffuse hump (oriented mesomorphic form) as well as scattering peaks of the $\{hk0\}$ reflections (oriented α-form). Along the diagonal axis, a bright peak was observed centered at $2\theta = 21.5°$. The off-axis diagonal scattering was similar to those of ePP but with higher intensities. Upon stretching, the HS fraction exhibited oriented crystalline phases of the α-form as well as the mesomorphic form (crystalline phase transformation).

The crystalline anisotropy of HS was also analyzed by azimuthal plots integrated through an annulus centered at the (110) scattering peaks ($13.4° \leq 2\theta \leq 14.6°$). Unlike ePP, the azimuthal plots of the HS fraction only contained one set of scattering (along the equatorial axis), as shown in Figure 6b. Higher anisotropies appeared in HS compared to the whole ePP. At 100% strain, anisotropy of HS was clearly observed whereas the ePP showed only a moderate level of anisotropy. The anisotropy at 200% strain almost reached a saturation level as further stretching to 300% did not appreciably increase the anisotropy.

The relaxation properties investigated by WAXS exhibited a similar response to those of ePP. No relaxation was seen from the WAXS patterns after 1 h at 300% strain. When released from stress, the HS fraction displayed a different response than the whole ePP. Permanent crystalline orientation persisted in HS as observed from the WAXS residual anisotropy. The residual scattering peaks were crystalline arcs, different than the diffuse hump (blob) observed when the sample was under strain. The equatorial crystalline arcs de-

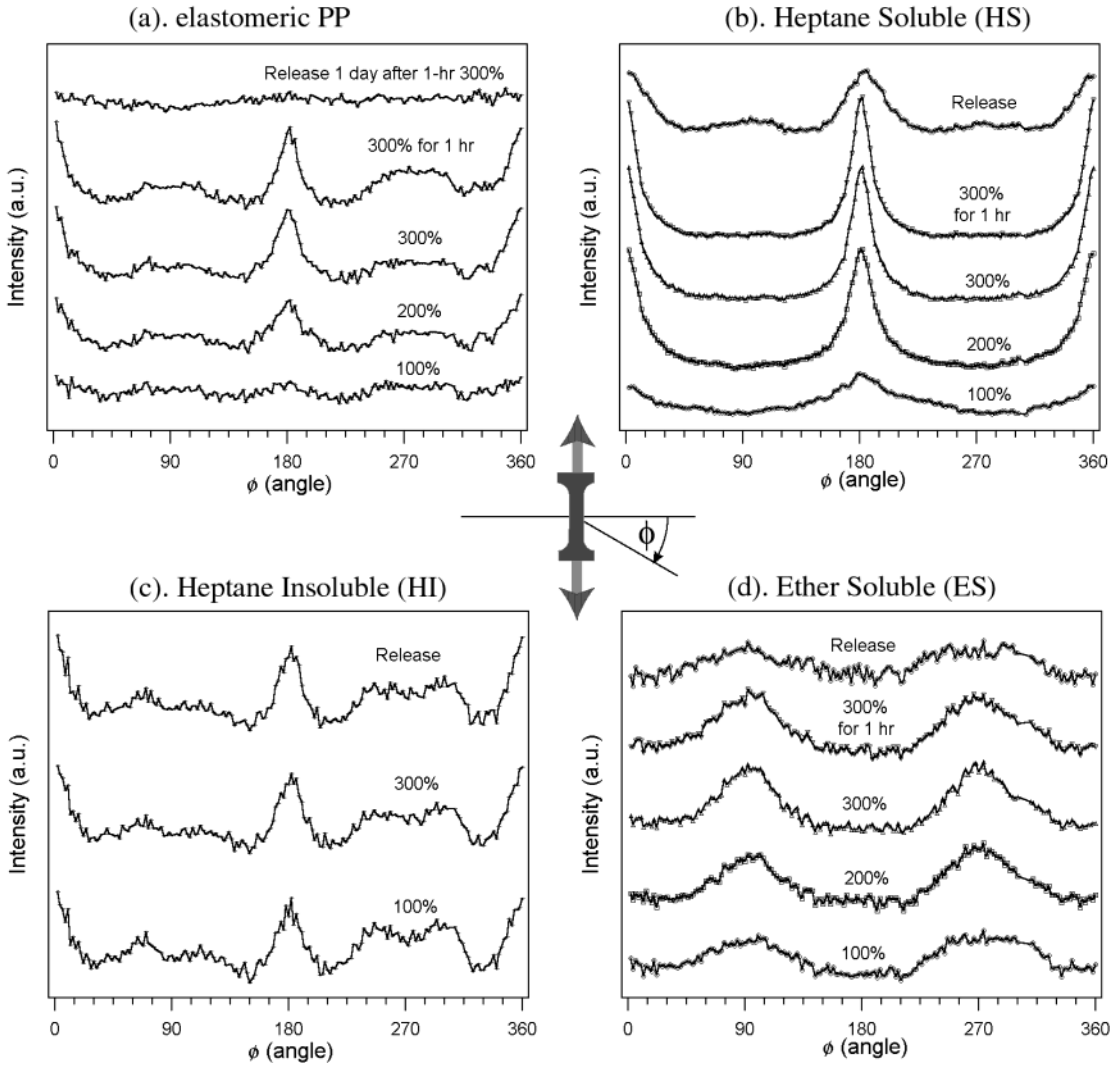

Figure 6. Azimuthal plots of integrated intensity for (a) ePP, (b) heptane-soluble fraction, (c) heptane-insoluble fraction, and (d) ether-soluble fraction. Integration was carried out at the (110) scattering reflection for (a), (b), and (c) and at the scattering arc for (d). Curves have been shifted vertically for clarity.

noted chains in the α-form crystals that were permanently oriented along the strain direction. The disappearance of the equatorial diffuse hump and the broadening of the off-axis diagonal peaks suggested some degree of reversibility of the mesomorphic form back to the α-form.

Long-range ordering was examined with small-angle X-ray scattering (SAXS). SAXS results for unstretched HS displayed an isotropic scattering pattern typical of semicrystalline materials. At 300% strain, SAXS showed a broad scattering peak along the meridian axis. For HS, the long-range anisotropy under 300% strain was similar to that obtained after the application of a strain of 300% for 1 h and released for 1 day, which is shown in Figure 8. The azimuthal intensity plot, integrated in the range $0.46 \leq q \leq 0.80$ nm^{-1}, showed a broad scattering peak centered along the meridian axis. The meridional scattering peak implied the presence of lamellae oriented with a preferred direction orthogonal to the strain axis (under strain and released from strain). The release of strain caused the maximum scattering peak to shift to a higher scattering vector (smaller *d*-spacing). The shift in the scattering peak suggested that amorphous chains between the lamellae relaxed to some extent upon the release of stress. Long-range ordering with *d*-spacings centered at 11.3 and 10.0 nm is evident for HS held at 300% strain and after released from stress, respectively.

2. Heptane-Insoluble (HI) Fraction. WAXS results of the tensile deformation of HI are presented in Figure 9. Similar to the whole ePP and HS, unstretched HI showed isotropic scattering rings typical of the α-phase isotactic PP.[40] Compared to the lower tacticity fractions, the scattering rings of the HI were more prominent, as expected from its higher tacticity. The WAXS response of HI upon stretching showed similarities to those of the HS fraction. A bright diffuse hump developed along the equatorial axis, the intensity of which increased with increasing strain. As shown in Figure 6c, the {110} azimuthal plots of HI under deformation exhibit a weak meridional scattering similar to that commonly observed [*a**] chain packing of the α-form isotactic PP.[53,54] The off-axis diagonal scattering, similar to those seen in HS, also occurred in HI but with lower intensity. As in the ePP and HS fraction, the crystalline anisotropy did not change appreciably during 1 h relaxation at 300%. Permanent deformation of HI, as probed by WAXS, appeared to show plastic behavior in that no relaxation was observed after releasing from stress.

3. Ether-Soluble (ES) Fraction. Figure 10 contains the response of the low-tacticity fraction as probed by WAXS. The unstretched ES exhibited an isotropic

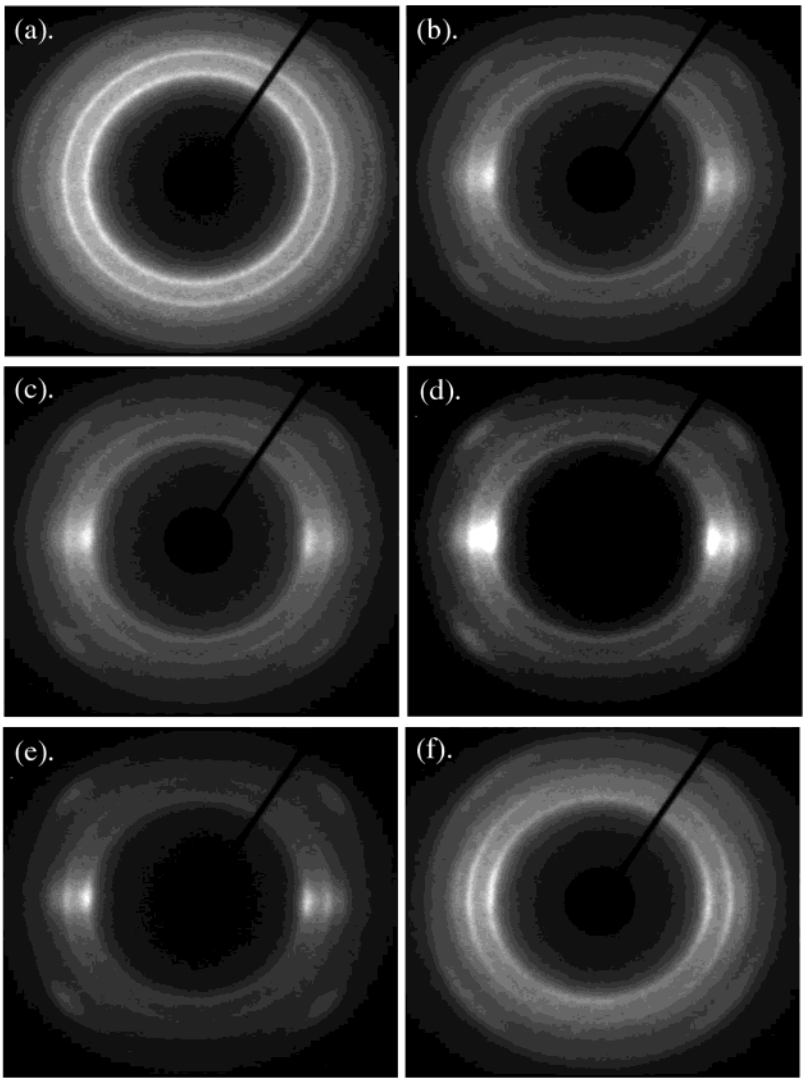

Figure 7. 2-D WAXS patterns of the intermediate-tacticity (HS) fraction: (a) unstretched, (b) at 100% strain, (c) at 200%, (d) at 300%, (e) at 300% after 1 h relaxation, (f) after a relaxation for 1 h at 300% strain and a stress-free period for 1-day. The strain axis is vertical.

scattering halo typical of an amorphous material. Upon stretching, crystalline arc with *d*-spacing of 0.551 ± 0.02 nm ($2\theta = 16.0°$) appeared with their center along the meridian axis. Figure 10c displays the 2-D WAXS pattern of ES at 300% strain after subtracting the amorphous background of the unstretched sample. The scattering peak coincided with the dominant crystalline peak of the β-form with *d*-spacing of 0.553 nm ($2\theta = 16.1°$). However, the second characteristic β-form crystalline peak with *d*-spacing of 0.417 nm ($2\theta = 21.2°$) was not found in the stretched ES.[49] The development of anisotropy with strain is illustrated in the azimuthal plots shown in Figure 6 through an integration of the first-order crystalline scattering ($15.2° \leq 2\theta \leq 16.8°$). These plots revealed that chains in the crystalline domains were oriented with a preferred direction orthogonal to the applied strain (shifted 90° from the primary peaks of ePP, HS, and HI). WAXS also showed that the crystallites did not relax when held at 300% strain for 1 h. Upon releasing from stress, the ES fraction relaxed as observed from the decreased peak intensity.

As reported in part 2 of the series, the rheooptical birefringence response of the ES sample was positive during stretching and became negative during stress relaxation. The negative birefringence implied that on average chains were oriented orthogonal to the strain axis, which is in agreement with the meridional arc observed in WAXS. Thermal investigation of the negative birefringence showed that the negatively birefringent crystallites melted near 75 °C.

Discussion

Rheooptical birefringence and WAXS show that both amorphous chains and crystallites in ePP are oriented in response to an external stress (Figures 2 and 5). WAXS data contain anisotropy arising from crystallites while the positive birefringence originates from both oriented amorphous chains and crystallites. As expected, the degree of orientation increases with increasing deformation. WAXS reveals three sets of scatterings in ePP, each denoting the type of crystalline orientation: an equatorial diffuse hump, an off-axis diagonal reflection, and a meridional arc. The scattering along the equatorial axis implies that the polymer chains are oriented parallel to the strain axis. The broad diagonal reflection and the equatorial diffuse hump suggest a crystalline phase transformation from the α-form to the mesomorphic form.[50] The unusual meridional arc is

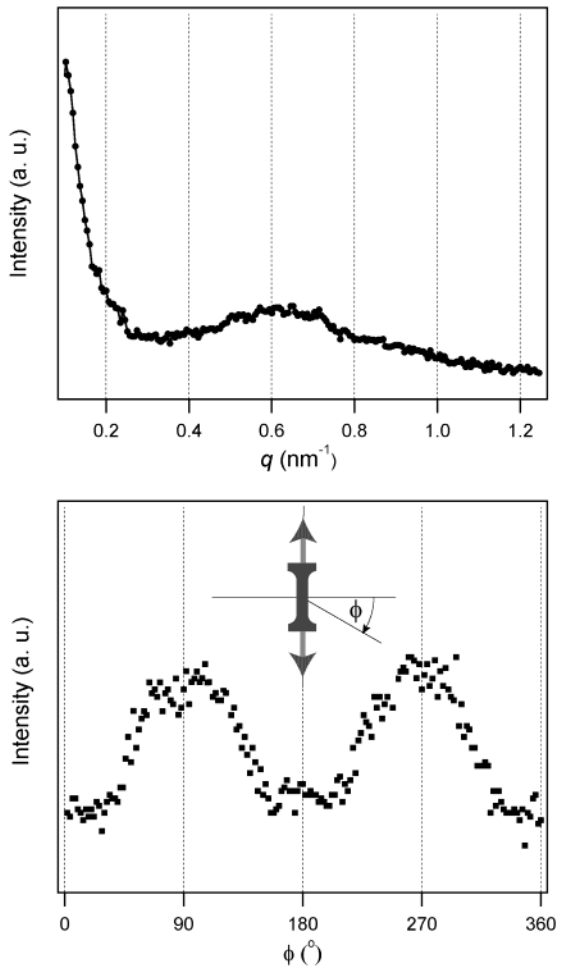

Figure 8. SAXS of the intermediate-tacticity (HS) fraction after 1 day released from 1 h of 300% strain: intensity scattering profile along the meridian axis (top) and azimuthal intensity profile (bottom).

indicative of crystalline chains preferentially oriented orthogonal to the strain direction.

The analysis of neat solvent fractions provides insight into the role of each solvent fraction in the ePP in response to deformation. Tensile experiments indicate that the low-tacticity ES behaves like a weak gum elastomer, whereas the high-tacticity HI shows plastic deformation. Only the intermediate-tacticity HS exhibits elastomeric behavior. WAXS results offer additional information from a molecular viewpoint: the unstretched HS and HI crystallize in the α-form isotactic PP, similar to ePP.[40,49] WAXS data also indicate that HI undergoes plastic deformation as no relaxation was observed after it was released from the stress field. Under similar conditions, the HS fraction exhibits some reversible crystalline anisotropy. In terms of crystalline reflections, as determined by WAXS, the intermediate- (HS) and high-tacticity (HI) fractions give rise to the observed equatorial diffuse hump and the off-axis diagonal scattering. The low-tacticity (ES) fraction, on the other hand, only displays meridional arc. From these observations, the contribution of each fraction in ePP can be identified. HS and HI are responsible for both the equatorial and off-axis diagonal scatterings, while the low-tacticity ES enhances the meridional arc.

Crystalline Phase Transformation. The diffuse equatorial hump and the off-axis diagonal scattering in the whole ePP, HS, and HI under stretching are fingerprints of the mesomorphic form of isotactic PP.[50] The four distinct diagonal reflections indicate that the mesomorphic form maintains a 3-fold helical conformation, as confirmed by many earlier studies.[49,51,55−57] We believe the deformation-induced crystalline transformation is due to crystalline phase conversion from the α-form or its defective form. The applied stress destroys the α-form crystalline structure (or its defects) and pulls the chains into the mesomorphic form with random helical hands (left or right). Similar behavior has also been reported by Hsiao and co-workers on the deformation of isotactic polypropylene fibers.[51] The authors reported the amount of mesomorphic form increased with increasing strain, as observed from the increase in intensity of the off-axis diagonal peaks.

Comparison of the stretched HS and HI allows an analysis of the crystalline phase transformation as a function of tacticity and crystallinity. Qualitatively, the HS fraction undergoes a higher amount of crystalline phase transformation to the mesomorphic form compared to the HI fraction. We believe that the higher amount of crystalline phase transformation is due to a higher number of defects in the HS than that in the HI fraction. When subjected to deformation, the chains with higher defects are more susceptible to crystalline transformation to the less-ordered mesomorphic form.

Lamella Deformation Model. The deformation behavior of the HS can be explained using the model proposed by Schultz on stretched polyethylene.[58] Crystalline phase transformation arises during the development of the lamellae orientation following the stages shown in Figure 11.[51] In the first stage of deformation at low strains, almost all of the strain is accommodated by the interlamellar amorphous chains aligning with the strain axis. At this stage, the lamellar ribbons slip rigidly past each other. The energy provided by the stress is not sufficient to deform the crystallites, but the chains in the amorphous phase can be oriented between lamellae. At higher strain when the tied chains are highly extended, deformation occurs by the slip-tilting of the crystalline lamellae. Chains packed in the lamellae are aligned with the strain direction, in agreement with that observed in WAXS. The chain alignment may destroy the crystalline α-form and convert the α-form crystallites to the mesomorphic form. At even higher strain, the lamellar ribbons are ruptured by blocks of crystals pulled out of the ribbons. The large energy provided by the strain is able to pull the helical chains in the crystal to become stretched helical chains, which may be aggregated into bundles with no specific arrangement of helical hands (mesomorphic form). The blocks from the same lamellae are still attached to each other by their side chains. At a very high strain, the blocks of ruptured lamellae become individual smaller blocks with minimal interactions between blocks. The lamellae are preferentially oriented orthogonal to the strain direction, in agreement with the observed weak meridional peak of SAXS.

Orthogonally Oriented Crystalline Chains. As is elaborated in part 2 of this series, the low-tacticity ES exhibits unusual deformation properties. The unstretched ES, with tacticity [mmmm] = 21%, shows properties typical of an amorphous material. WAXS and DSC show a very low amount of crystallinity (1−2%) and do not show evidence of any increase in crystallinity after annealing at 120 °C for 6 h.[40] The observed crystallization of ES occurs under both tensile stretching

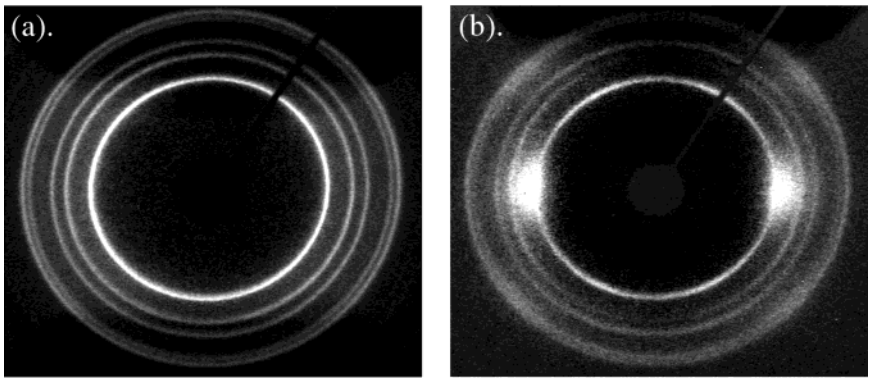

Figure 9. 2-D WAXS patterns of the high-tacticity (HI) fraction: (a) before stretching and (b) at 300% strain with vertical strain axis.

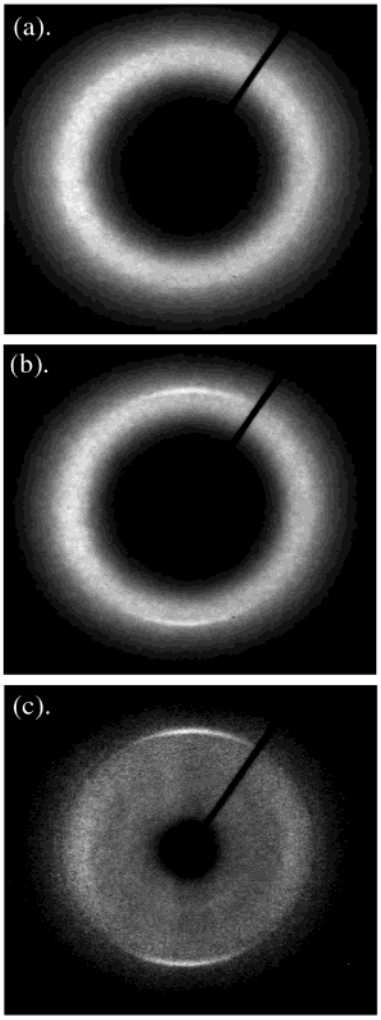

Figure 10. 2-D WAXS images of the low-tacticity (ES) fraction with strain axis along the vertical direction: (a) unstretched, (b) at 300% strain, and (c) at 300% strain after subtraction of the unstretched scattering pattern.

and step-shear deformations. Rheooptical birefringence and WAXS independently confirm that crystalline chains are oriented orthogonal to the strain direction. The crystallization of the low-crystallinity ES (1−2% by DSC and WAXS) implies there exist crystallizable isotactic sequences to accommodate crystallization. The isotactic sequence lengths must be sufficiently long to allow crystallization, but concurrently the overall tacticity of the chains must be low to maintain solubility in boiling diethyl ether.

The crystalline form of the neat ES under deformation is not fully understood. As displayed in Figure 10, the meridional arc occurs at scattering angle $2\theta = 16.0°$ that coincides with the first characteristic reflection of the β-form isotactic PP. However, the second smaller peak characteristic of the β-form is not observed. When the ES is blended with higher isotacticity fractions, as in the parent ePP, the meridional arc is increased by a large amount. However, the meridional arc occurs at $2\theta = 14.0°$, corresponding to the (110) reflection of the α-form. The same behavior is also observed in the ES/HI blend as reported in part 2. The different crystalline reflection of the neat ES as compared to the parent ePP and ES/HI blend shows that ES possesses different crystalline growth mechanisms when it is in its neat form and when it is blended with the α-form isotactic PP. These results suggest that when ES is blended with higher-tacticity chains, it can cocrystallize with the α-form crystals (see part 2).

Relaxation Dynamics and Tensile Set. The relaxation dynamics of ePP when held at constant strain was monitored by tensile stress, birefringence, and WAXS. Simultaneous stress−birefringence experiments showed that both quantities decayed over time when held at constant strain. The faster relaxation of birefringence compared to the tensile stress (Figure 2) suggests that the stress relaxation is primarily due to the relaxation of amorphous chains. Both oriented amorphous chains and crystallites contribute to the birefringence. We believe the plateau in birefringence is attributed to oriented amorphous chains as well as oriented crystallites. WAXS results, as shown in Figures 5 and 6, confirm that relaxation occurs primarily from amorphous chains, as the crystalline anisotropy does not decay significantly during stress relaxation. Qualitative assessment of the amount of crystallinity during constant strain does not indicate any increase. The number of oriented chains, either in crystallites or pinned within the crystalline network, increases with increasing strain as shown by the increase in the stress and birefringence plateaus with increasing strain (Figure 3).

As exhibited in Figures 2 and 4, the tensile set, expressed as residual strain, correlates with the residual birefringence of the sample at zero stress. The residual birefringence implies that chains are not fully relaxed to an isotropic state. We believe the permanent deformation arises from immobile oriented crystalline chains and "trapped" amorphous chains between the deformed crystalline networks. The permanent anisotropy that remains without an applied stress is dependent on strain history, as shown in Figure 4. The longer

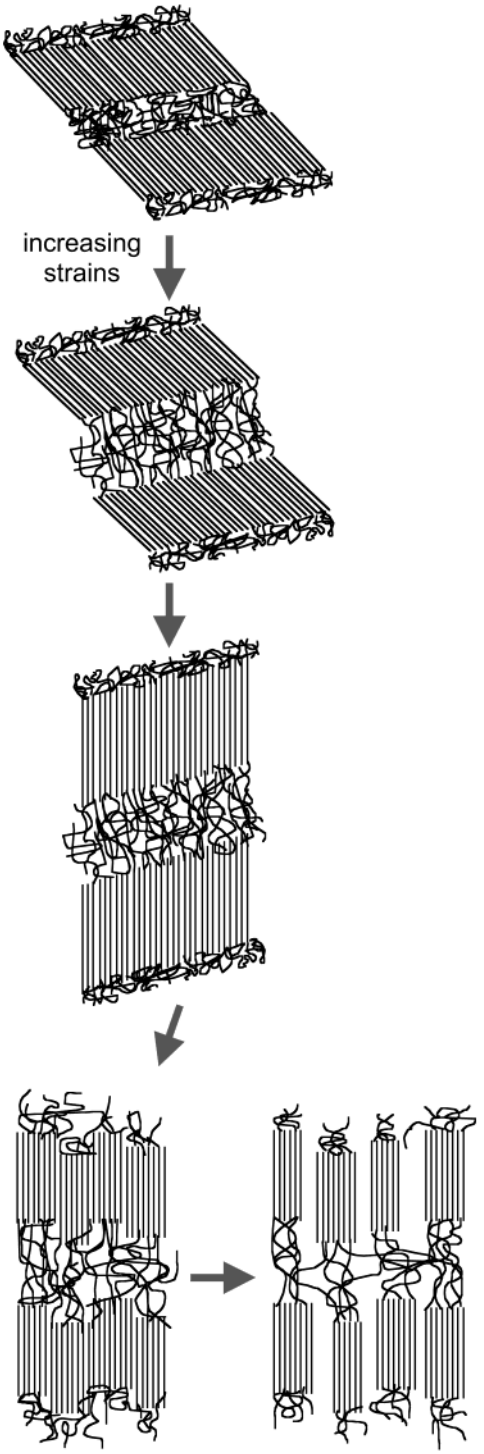

Figure 11. Lamellar deformation model adopted from Schultz.[58]

a sample is held under strain, the more crystallites and amorphous chains are permanently oriented. This suggests that at room temperature ePP chains have high enough chain mobility to reorient in response to external stresses. The observation is similar to the heat-setting process in oriented structures.

Conclusions

Tensile stress, rheooptical birefringence, and X-ray scattering studies of the elastomeric polypropylene (ePP) produced by 2-arylindene catalysts provide insight into the dynamic response and the origin of tensile set within these materials. Tensile stretching of ePP causes both amorphous chains and crystallites to orient in response to the stress field. WAXS shows that crystallites not only are oriented but also undergo crystalline phase transformation from the α-form to the mesomorphic form. Stress relaxation occurs primarily due to the amorphous chains that are not pinned within the crystalline networks. When ePP is free from stress, the imperfect elasticity originates from the permanent orientation of the crystallites and amorphous chains that are pinned within the crystalline network.

WAXS studies of each solvent fraction comprising the ePP (ES, HS, and HI) reveal the contribution of each solvent fraction in the whole ePP. High-tacticity fractions (HS and HI) undergo crystalline phase transformation from the α-form to the mesomorphic form under deformation. The low-tacticity ES fraction contains crystalline chains preferentially aligned orthogonal to the strain direction. In a deformed ePP matrix, the ES fraction forms crystallites of the α-form isotactic PP. Neat ES undergoes a different deformation model, and the type of crystalline form produced is not conclusive, although the observed WAXS crystalline reflection suggests a β-form crystalline phase.

Acknowledgment. G.G.F. and R.M.W. acknowledge support from the National Science Foundation (DMR-9910386). We acknowledge the support of the Stanford Synchrotron Radiation Laboratory in providing facilities used in these experiments: this work was supported by Department of Energy Contract DE-AC03-76SF00515. W.W. thanks Holger Schönherr for fruitful discussion on the subject.

References and Notes

(1) Brintzinger, H. H.; Fischer, D.; Mulhaupt, R.; Rieger, B.; Waymouth, R. M. *Angew. Chem., Int. Ed. Engl.* **1995**, *34*, 1143−1170.
(2) Fink, G.; Mülhaupt, R.; Brintzinger, H. H. *Ziegler Catalysts: Recent Scientific Innovations and Technological Improvements*; Springer-Verlag: Berlin; New York, 1995.
(3) Resconi, L.; Cavallo, L.; Fait, A.; Piemontesi, F. *Chem. Rev.* **2000**, *100*, 1253−1345.
(4) Ewen, J. A. *Macromol. Symp.* **1995**, *89*, 181−196.
(5) Ewen, J. A.; Elder, M. J.; Jones, R. L.; Haspeslagh, L.; Atwood, J. L.; Bott, S. G.; Robinson, K. *Makromol. Chem., Macromol. Symp.* **1991**, *48*−*9*, 253−295.
(6) Kaminsky, W.; Sinn, H. *Transition Metals and Organometallics as Catalysts for Olefin Polymerization*; Springer-Verlag: Berlin; 1988.
(7) Keii, T.; Soga, K. *Catalytic Olefin Polymerization: Proceedings of the International Symposium on Recent Developments in Olefin Polymerization Catalysts, Tokyo, October 23*−*25, 1989*; Elsevier: New York, 1990.
(8) Coates, G. W.; Waymouth, R. M. *Science* **1995**, *267*, 217−219.
(9) Kaminsky, W.; Buschermoehle, M. *NATO ASI Ser., Ser. C* **1987**, *215*, 503−514.
(10) Hu, Y. R.; Krejchi, M. T.; Shah, C. D.; Myers, C. L.; Waymouth, R. M. *Macromolecules* **1998**, *31*, 6908−6916.
(11) Natta, G.; Mazzanti, G.; Crespi, G.; Moraglio, G. *Chim. Ind.* **1957**, *39*, 275−283.
(12) Natta, G. *J. Polym. Sci.* **1959**, *34*, 531−549.
(13) Collette, J. W.; Ovenall, D. W.; Buck, W. H.; Ferguson, R. C. *Macromolecules* **1989**, *22*, 3858−3866.
(14) Collette, J. W.; Tullock, C. W. U.S. Patent 4,335,225, 1982.
(15) Collette, J. W.; Tullock, C. W.; MacDonald, R. N.; Buck, W. H.; Su, A. C. L.; Harrel, J. R.; Mulhaupt, R.; Anderson, B. C. *Macromolecules* **1989**, *22*, 3851−3858.
(16) Mallin, D. T.; Rausch, M. D.; Lin, Y. G.; Dong, S.; Chien, J. C. W. *J. Am. Chem. Soc.* **1990**, *112*, 2030−2031.

(17) Llinas, G. H.; Dong, S. H.; Mallin, D. T.; Rausch, M. D.; Lin, Y. G.; Winter, H. H.; Chien, J. C. W. *Macromolecules* **1992**, *25*, 1242−1253.
(18) Chien, J. C. W.; Llinas, G. H.; Rausch, M. D.; Lin, Y. G.; Winter, H. H.; Atwood, J. L.; Bott, S. G. *J. Polym. Sci., Part A: Polym. Chem.* **1992**, *30*, 2601−2617.
(19) Gauthier, W. J.; Corrigan, J. F.; Taylor, N. J.; Collins, S. *Macromolecules* **1995**, *28*, 3771−3778.
(20) Gauthier, W. J.; Collins, S. *Macromolecules* **1995**, *28*, 3779−3786.
(21) Gauthier, W. J.; Collins, S. *Macromol. Symp.* **1995**, *98*, 223−231.
(22) Chen, R.; Xie, M. R.; Wu, Q.; Lin, S. G. *J. Polym. Sci., Part A: Polym. Chem.* **2000**, *38*, 411−415.
(23) Kuhl, O.; Koch, T.; Somoza, F. B.; Junk, P. C.; Hey-Hawkins, E.; Plat, D.; Eisen, M. S. *J. Organomet. Chem.* **2000**, *604*, 116−125.
(24) Longo, P.; Amendola, A. G.; Fortunato, E.; Boccia, A. C.; Zambelli, A. *Macromol. Rapid Commun.* **2001**, *22*, 339−344.
(25) Mansel, S.; Perez, E.; Benavente, R.; Perena, J. M.; Bello, A.; Roll, W.; Kirsten, R.; Beck, S.; Brintzinger, H. H. *Macromol. Chem. Phys.* **1999**, *200*, 1292−1297.
(26) Nedorezova, P. M.; Tsvetkova, V. I.; Bravaya, N. M.; Savinov, D. V.; Optov, V. A. *J. Polym. Sci., Ser. A* **2000**, *42*, 573−579.
(27) Schmidt, R.; Alt, H. G. *J. Organomet. Chem.* **2001**, *621*, 304−309.
(28) Yoon, J. S.; Lee, Y. S.; Park, E. S.; Lee, I. M.; Park, D. K.; Jung, S. O. *Eur. Polym. J.* **2000**, *36*, 1271−1275.
(29) Resconi, L.; Piemontesi, F.; Lin-Chen, Y. U.S. Patent 5,747,621, 1998.
(30) Sassmannshausen, J.; Bochmann, M.; Rosch, J.; Lilge, D. *J. Organomet. Chem.* **1997**, *548*, 23−28.
(31) Chien, J. C. W.; Iwamoto, Y.; Rausch, M. D.; Wedler, W.; Winter, H. H. *Macromolecules* **1997**, *30*, 3447−3458.
(32) Bravakis, A. M.; Bailey, L. E.; Pigeon, M.; Collins, S. *Macromolecules* **1998**, *31*, 1000−1009.
(33) Dietrich, U.; Hackmann, M.; Rieger, B.; Klinga, M.; Leskelae, M. *J. Am. Chem. Soc.* **1999**, *121*, 4348−4355.
(34) Kukral, J.; Lehmus, P.; Feifel, T.; Troll, C.; Rieger, B. *Organometallics* **2000**, *19*, 3767−3775.
(35) Pellon, B. J.; Allen, G. C. Eur. Pat. Appl. 0 475 306 A1, 1992.
(36) Hauptman, E.; Waymouth, R. M.; Ziller, J. W. *J. Am. Chem. Soc.* **1995**, *117*, 11586−11587.
(37) Kravchenko, R.; Masood, A.; Waymouth, R. M. *Organometallics* **1997**, *16*, 3635−3639.
(38) Kravchenko, R.; Masood, A.; Waymouth, R. M.; Myers, C. L. *J. Am. Chem. Soc.* **1998**, *120*, 2039−2046.
(39) Hu, Y. R.; Carlson, E. D.; Fuller, G. G.; Waymouth, R. M. *Macromolecules* **1999**, *32*, 3334−3340.
(40) Schonherr, H.; Wiyatno, W.; Pople, J. A.; Frank, C. W.; Fuller, G. G.; Gast, A. P.; Waymouth, R. M. *Macromolecules* **2002**, *35*, 8498−8508.
(41) Roe, R. J. *Methods of X-ray and Neutron Scattering in Polymer Science*; Oxford University Press: New York, 2000.
(42) Chu, B.; Hsiao, B. S. *Chem. Rev.* **2001**, *101*, 1727−1761.
(43) Wiyatno, W.; Chen, Z.-R.; Liu, Y.; Waymouth, R. M.; Krukonis, V.; Brennan, K., submitted to *Macromolecules* .
(44) Fuller, G. G. *Optical Rheometry of Complex Fluids*; Oxford University Press: New York, 1995.
(45) The 2θ values presented in this paper use a standard X-ray source (Cu Kα) wavelength of 1.54 Å instead of the actual wavelength of the synchroton source.
(46) Wiyatno, W.; Pople, J. A.; Gast, A. P.; Waymouth, R. M.; Fuller, G. G., submitted to *Macromolecules*.
(47) Janeschitz-Kriegl, H. *Polymer Melt Rheology and Flow Birefringence*; Springer-Verlag: Berlin, 1983.
(48) Wales, J. L. S. *The Application of Flow Birefringence to Rheological Studies of Polymer Melts*; Delft University Press: Delft, 1976.
(49) Moore, E. P. *Polypropylene Handbook: Polymerization, Characterization, Properties, Processing, Applications*; Hanser/Gardner Publications: New York, 1996.
(50) Wyckoff, H. W. *J. Polym. Sci.* **1962**, *62*, 83−114.
(51) Ran, S. F.; Zong, X. H.; Fang, D. F.; Hsiao, B. S.; Chu, B.; Phillips, R. A. *Macromolecules* **2001**, *34*, 2569−2578.
(52) Decandia, F.; Iannelli, P.; Staulo, G.; Vittoria, V. *Colloid Polym. Sci.* **1988**, *266*, 608−613.
(53) Samuels, R. J. *Structured Polymer Properties: The Identification, Interpretation, and Application of Crystalline Polymer Structure*; John Wiley & Sons: New York, 1974.
(54) Fujiyama, M.; Wakino, T.; Kawasaki, Y. *J. Appl. Polym. Sci.* **1988**, *35*, 29−49.
(55) Gomez, M. A.; Tanaka, H.; Tonelli, A. E. *Polymer* **1987**, *28*, 2227−2232.
(56) Corradini, P.; Derosa, C.; Guerra, G.; Petraccone, V. *Polym. Commun.* **1989**, *30*, 281−285.
(57) Martorana, A.; Piccarolo, S.; Scichilone, F. *Macromol. Chem. Phys.* **1997**, *198*, 597−604.
(58) Schultz, J. M. *Polymer Materials Science*; Prentice Hall: Englewood Cliffs, NJ, 1974.

MA020261O